

## **Morphology of electrospun poly(ethylene oxide) ultra-fine fibres with incorporated MoO<sub>3</sub> nanoparticles**

Mahnaz Shafiei<sup>1,2,\*</sup>, Ibrahim El-chami<sup>2</sup>, Llew Rintoul<sup>1</sup>, Behraad Bahreyni<sup>2,\*</sup>

<sup>1</sup>Institute for Future Environments and School of Chemistry, Physics, and Mechanical Engineering,  
Queensland University of Technology (QUT), Brisbane, Australia;

<sup>2</sup>School of Mechatronic Systems Engineering, Simon Fraser University, Surrey, Canada

\*Corresponding authors' Email: mahnaz.shafiei@qut.edu.au; behraad@ieee.org

### **Abstract**

N-type semiconducting molybdenum trioxide (MoO<sub>3</sub>) nanoparticles embedded in polyethylene oxide (PEO) polymer ultra-fine fibres were deposited directly onto silicon substrates using an electrospinning technique. The effects of different MoO<sub>3</sub>/PEO concentrations as well as electrospinning parameters on the fibre morphologies were examined. Experimental results show that embedding nanoparticles and electrospinning onto small areas can be achieved without use of solvents or transfer of the deposited nanostructures. This approach offers a cost effective fabrication method to produce a diverse range of multifunctional materials for many applications including electronics, mechanical enhancement, drug delivery and gas sensing.

**Keywords:** Electrospinning; MoO<sub>3</sub> Nanoparticles (NPs); Poly(Ethylene Oxide); FESEM; TEM; FT-IR.

## 1. Introduction

One dimensional (1D) nanostructures in the form of wires, belts, rods, tubes and fibres have been extensively utilized in different electrochemical, optical, and bio-sensing applications [1-8]. The increase in demand for these nanostructures is mainly attributed to their unique electrical, optical, magnetic, thermal, mechanical and chemical properties [5, 9]. Several fabrication methods including electrochemical deposition [10], electroless deposition [11], sol-gel [12], chemical vapour deposition (CVD) [13, 14], and atomic layer deposition (ALD) [15] have been utilized to deposit 1D carbon [13, 14], metal [15], oxide [12], semiconducting [12], polymer [10], and hybrid [11] nanostructures. However, the CVD and ALD processes require high deposition temperatures, typically ranging between 500 °C and 900 °C. In addition, the required pre-processing steps (e.g., generation of nucleation sites) add to process complexity.

Other deposition processes like sol-gel, electroless, and electrochemical depositions require the substrate to be immersed in an aqueous solution for a deposition process. Immersion in aqueous solutions makes the synthesis of nanostructures incompatible with many fabrication processes for microsystems [11]. On the other hand, electrospinning, a versatile and cost effective deposition method has demonstrated the capacity to deposit ultrafine fibres of different materials (such as polymers, metals, metal-oxides and composites) with diameters ranging from a few tens of nanometers to a few microns in various fibrous assemblies including mixed nanocomposite, double-layers, core-shell or hollow [5, 9, 16-19].

Recently, incorporating functional nanoparticles (NPs) with electrospun fibres has attracted considerable attention in several multidisciplinary research fields [5, 20]. Zhang and Yu have recently reviewed NPs-electrospun fibre composite fabrications and their applications [5]. NPs-electrospun fibres significantly improve different physical and chemical perturbation properties of the electrospun fibres/mats. On the other hand, electrospun fibres/mats could preserve NPs from corrosion and/or oxidation, especially for NPs with anisotropic structures [5].

There are two major methods for producing electrospun NP fibres [5]. Indirect synthesis is used when NPs are not well dispersed within the solution used for electrospinning. Hence, post-processing treatments such as surface treatment [21, 22], hydrothermal [23, 24], or gas–solid reaction [25] are required to incorporate NPs into the electrospun fibres. Based on different post-treatment methods, the NPs can be formed on the surfaces or embedded within the fibres. Direct synthesis of electrospun NP fibres occurs when uniformly distributed NPs in polymer solution are electrospun to produce composite fibres. The properties of the composites can be easily engineered by controlling the concentration of the NPs within the polymer fibres. In addition, the NPs are not notably deformed nor affected by the electrospinning process, making this method much more versatile than indirect synthesis [5].

Molybdenum trioxide ( $\text{MoO}_3$ ) is a wide bandgap n-type semiconductor. The nanostructured form of this material has shown great potential in different applications including as a catalyst [26], in large-area display devices [27], as gas sensors [6-8, 28], and as batteries [29]. According to the literature, a few research groups have developed electrospun  $\text{MoO}_3$  nanofibres using different precursors and polymers [29-32]. Gouma et al. produced an electrospun mat of  $\text{MoO}_3$  nanofibres using molybdenum oxide sol dissolved in n-butanol and solutions of polyvinylpyrrolidone (PVP) and polyethylene oxide (PEO) polymers in ethanol and water. They obtained aligned encapsulation of  $\text{MoO}_3$  nanowires with diameter of the order of 10-50 nm inside the polymeric fibre [31, 32]. Li et al. used a solution of polyvinyl alcohol (PVA)/ammonium molybdate composite in water and ethanol to produce  $\text{MoO}_3$  nanofibres. The diameter of the electrospun PVA/ammonium molybdate composites were 400-600 nm. After calcination at 500 °C, nanofibres of  $\text{MoO}_3$  with diameters of 100-150 nm were obtained. Calcination at temperatures above 500 °C resulted in the formation of  $\text{MoO}_3$  nanoplatelets [30].

Feng et al. reported electrospinning of  $\text{MoO}_3$ /carbon composite using a solution of  $(\text{NH}_4)_2\text{MoO}_4$ /polyacrylonitrile (PAN) in dimethylformamide (DMF). Calcination of the electrospun composite in Ar resulted in porous structures on the fibres, while calcination in air caused formation

of MoO<sub>3</sub> nanoplatelets [29]. In all these reports, an organic solvent was used for the electrospinning solution. In addition, the electrospun fibres were dispersed in an organic solvent in order to be transferred onto a small substrate for subsequent applications. This article, on the other hand, presents a simple and cost-effective one-step process without using any organic solvent to electrospin MoO<sub>3</sub> NPs fibres directly onto a small area with a controlled and selective deposition area.

In this work, several solutions of PEO and MoO<sub>3</sub> in deionized (DI) water at different concentrations were prepared and electrospun. Different electrospinning parameters including solution concentration, distance between the needle and the collector, applied voltage, feeding rate and needle size were optimized in order to obtain quality nanofibres. The basic electrospinning setup was simply modified by using a multiple field technique in order to reduce and control the deposition area [33]. The PEO/MoO<sub>3</sub> NPs fibres were successfully electrospun directly onto small substrates without requiring an additional post-deposition transfer step. The materials properties of the electrospun PEO ultra-fine fibres with incorporated MoO<sub>3</sub> NPs were investigated using a range of analytical tools.

## **2. Experimental Section**

### **2.1. Sample Preparation**

PEO powder with molecular weight of 400,000 and MoO<sub>3</sub> powder (99.98% purity) purchased from Sigma Aldrich were mixed with distilled water as the solvent to prepare required solutions for the electrospinning experiments. Different PEO concentrations (10, 15, 17, 20 %w/v) were prepared by mixing 0.10, 0.15, 0.17 and 0.20 g of PEO in 1 ml of water. 0.01, 0.05, 0.07 and 0.10 g of MoO<sub>3</sub> powder were mixed with 1 ml of water to make 1, 5, 7, 10 w/v% concentrations. Each mixture was stirred for 1 h using a probe sonicator (SONICS, Vibra<sup>TM</sup>cell) with configuration of AMP - 40%, PULSE - 25 s ON/5 s OFF before a homogenous solution formed. The PEO and MoO<sub>3</sub> solutions were then mixed at different volume ratios ranging from 1 to 10 and electrospun on clean silicon

substrates and copper grids. A typical electrospinning setup used in this work comprised a high voltage (HV) source from Gamma High Voltage Research, Inc.; a syringe pump (NE-300) from New Era Pump Systems, Inc. and a 1 ml plastic syringe with a blunt metal needle. Different electrospinning parameters including solution concentration, distance between the needle and the collector, applied voltage, feeding rate and needle size as summarized in Table 1 were examined in order to obtain quality nanofibres. An optical microscope was utilized for rapid analysis of materials on substrates.

**Table 1.** Electrospinning parameters for synthesis of PEO nanofibres embedded with MoO<sub>3</sub> nanoparticles.

Sample	PEO Conc (w/v%)	MoO <sub>3</sub> Conc (w/v%)	VR (PEO:MoO <sub>3</sub> )	D (cm)	V (kV)	R (ml/h)	N (G)	Formation
1	10	1	1:1	10	~8.5	0.05	30	Droplets
2	10	1	2:1	8.5	9	0.10	30	Droplets
3	10	1	2:1	10	~7.5	0.30	30	Droplets
4	10	1	5:1	10	8	0.19	30	Droplets
5	10	5	10:1	10	16	0.10	23	Droplets
6	10	5	10:1	10	15	0.10	21	Droplets
7	10	5	10:1	10	14	0.10	21	Droplets
8	10	5	10:1	10	15	0.10	21	Droplets
<b>9</b>	<b>15</b>	<b>5</b>	<b>10:1</b>	<b>10</b>	<b>12</b>	<b>0.10</b>	<b>21</b>	<b>Beaded fibres</b>
10	17	5	10:1	10	12	0.10	21	Droplets
11	20	5	10:1	10	12	0.10	21	Droplets
<b>12</b>	<b>15</b>	<b>7</b>	<b>10:1</b>	<b>10</b>	<b>12</b>	<b>0.10</b>	<b>21</b>	<b>Beaded fibres</b>
<b>13</b>	<b>15</b>	<b>10</b>	<b>10:1</b>	<b>10</b>	<b>12</b>	<b>0.10</b>	<b>21</b>	<b>Beaded fibres</b>
Conc: w/v% concentration in DI water; VR: Volume ratio between PEO and MoO <sub>3</sub> ; D: Distance between needle and collector; V: Applied voltage; R: Feeding rate; N: Needle size								

## 2.2. Electrospinning

Electrospinning is a relatively simple technique which utilizes high electrostatic forces to produce fine fibres from polymer solutions. Due to surface tension forces, the solution forms small droplets at the needle tip as it is ejected at a controlled rate by the syringe pump. Applying high voltage between the needle and electrode builds up charge on the droplet surface. Eventually, electrostatic

repulsive forces due to charge build up overcome surface tension forces at the needle tip. Thus, a Talyor cone is formed, causing the liquid jet to stretch as it is deposited towards the ground collector. Fibres are formed as the solvent evaporates and solidified jets approach the electrodes at the collector [5, 9, 16-18].

The electrospinning process is governed by solution parameters including solution viscosity, polymer concentration, molecular weight, conductivity, and surface tension. In addition, the applied voltage, the distance between the needle tip and the collector, feeding rate, humidity, and temperature significantly influence the morphology and diameter of electrospun fibres. Therefore, proper optimization of these parameters is required to obtain nanofibres with desired morphology and diameters [5, 9, 16-18].

In order to control and reduce the deposition area of the fibres, we modified the multiple field technique proposed by Deitzel et al. [33]. Deitzel's group employed rings placed below the tip of the spinneret as auxiliary electrodes with a positive charge different from the voltage applied to the tip and a negative charge applied to the collector. In our setup, a metallic ring with diameter of  $R_t \sim 5$  cm was connected to the tip of the needle and another metallic ring with diameter of  $R_c \sim 4$  cm was mounted at a distance of 2 cm from the collector (Figure 1). The electrospinning parameters were optimized to obtain fibres. Voltages of +9.5 kV and +2.6 kV were applied to the tip of the needle (and ring  $R_t$ ) and  $R_c$ , respectively. The distance between the needle and collector was set to 6 cm and the feeding rate was optimized at 0.2 ml/h.

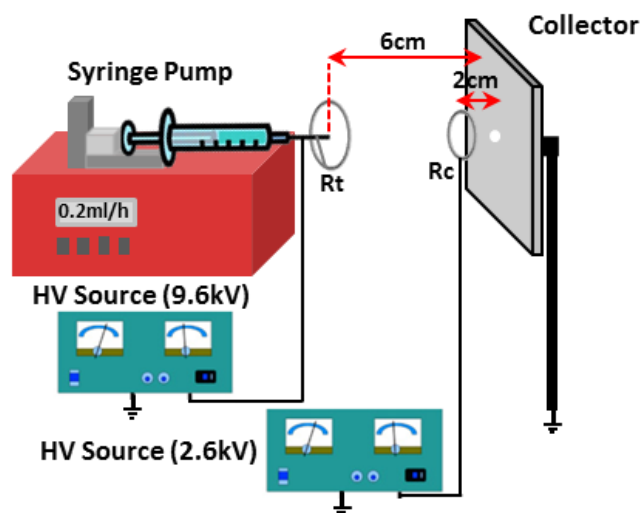


**Figure 1.** Schematic diagram of multi-field electrospinning setup.

### 2.3. Material Characterization

Structure, morphology and elemental composition of the electrospun nanofibres were analysed using field emission scanning electron microscopy (FEI Nova NanoSEM equipped with an energy dispersive X-ray detector) and a transmission electron microscope with an EDX detector (FEI Osiris) was used for STEM/EDX mapping. Fourier Transform infrared (FT-IR) spectra were measured on a Nicolet iS50 spectrometer, which incorporates a single bounce diamond ATR module with a dedicated deuterated triglycine sulfate DTGS detector (Thermo Fisher Scientific Inc., Madison, WI, USA). The samples, as deposited on the Si substrate were placed fibre-side down and pressed directly onto the diamond refractive element of the ATR crystal. Spectra were accumulated for 64 scans at a resolution of  $4\text{ cm}^{-1}$  across the region from  $4000\text{--}600\text{ cm}^{-1}$ . ATR correction and baseline subtractions were performed using Nicolet OMNIC V 9 software.

### 3. Results and Discussion

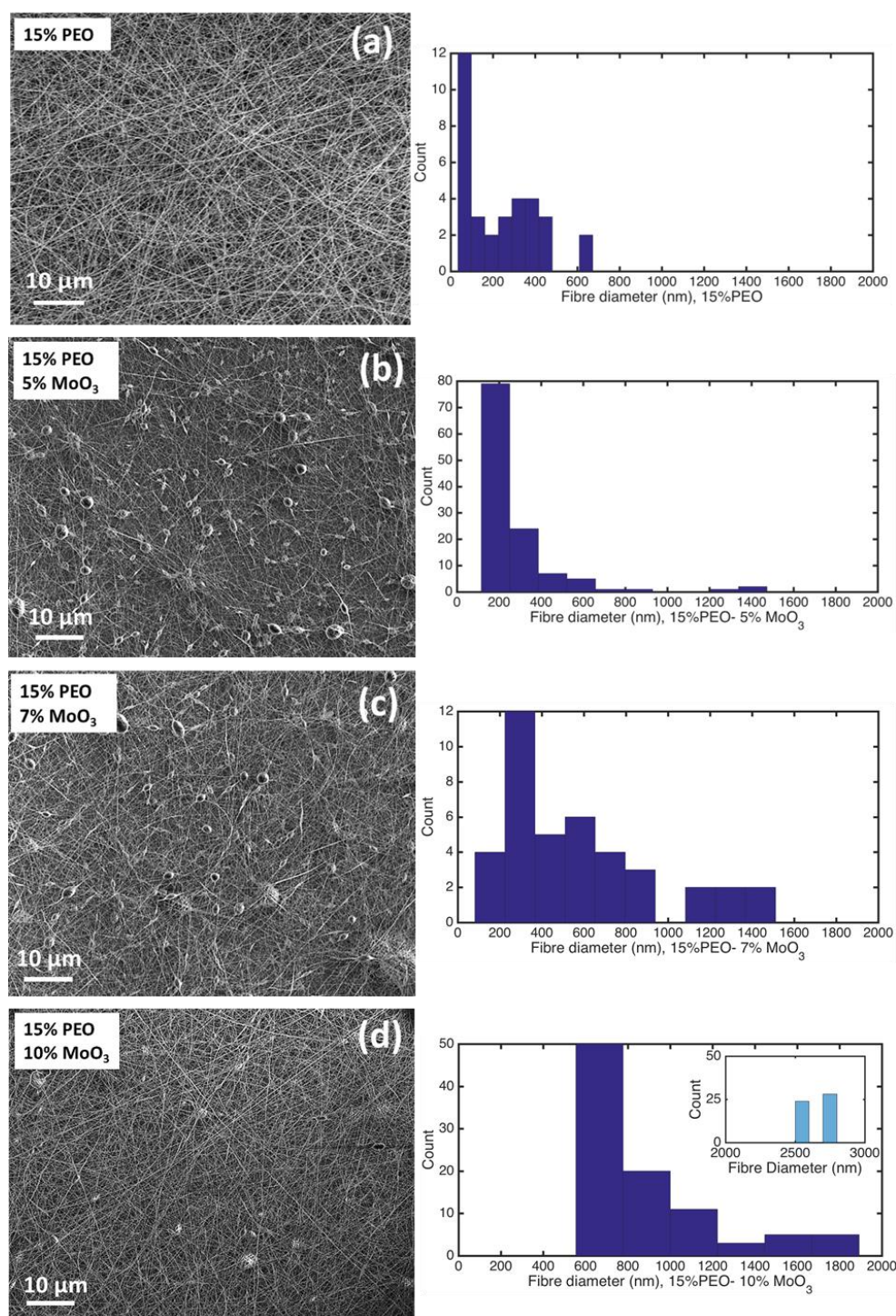
By optimizing the electrospinning deposition conditions (Table 1), beaded fibres were initially obtained by using 15% PEO and 5%  $\text{MoO}_3$  solutions with the parameters of 10 cm distance between needle tip and collector; 21 G needle; voltage of 12 kV, volume ratio of 10:1 for PEO: $\text{MoO}_3$  solutions and feeding rate of 0.1 mL/hr (Sample 9). One parameter that influences the

generation of beads is the solution concentration [34]. The viscosity and concentration of the solution play important roles in determining the fibre morphology during electrospinning. The viscosity of the solution is strongly related to solids concentration. It has been reported that with very high viscosity the ejection of jets from the polymer solution is difficult and also with very low viscosity, there is no continuous fibre formation [34]. Therefore, we investigated the effect of an increase in the concentrations of PEO and MoO<sub>3</sub> solutions on the generation of beads while other parameters for Sample 9 were kept constant.

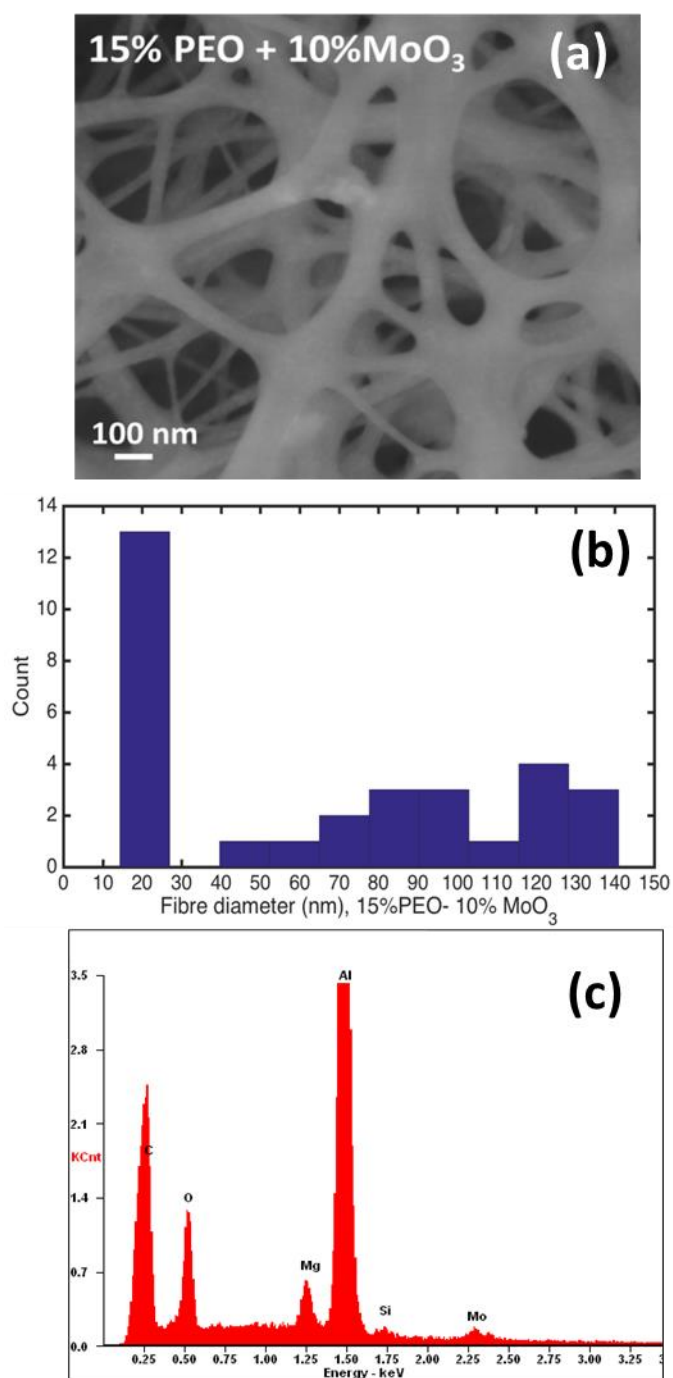
By increasing the PEO concentrations from 15% to 20%, fibres were not formed (Samples 10 and 11), while an increase in the concentration of MoO<sub>3</sub> resulted in a reduction of beads in the fibres (Samples 12 and 13).

Figure 2 shows FESEM micrographs of electrospun fibres of pure PEO and PEO with incorporated MoO<sub>3</sub> NPs using different concentrations of MoO<sub>3</sub> (5%, 7% and 10%). The deposition was performed for 2 min. As seen in Figure 2, there were fewer beads in the sample with higher concentrations of MoO<sub>3</sub> (10%). The histogram showing the size distribution of fibre diameters (right images of Figure 2) confirmed an increase in fibre diameter with increase of solution concentration [5, 20, 34].

A high magnification FESEM image of the sample with 10% MoO<sub>3</sub> (Figure 3a) shows a mesh with interconnected fibres. Figure 3b reveals electrospun fibres with different diameters in the range of 15-140 nm. The EDX analysis (Figure 3c) confirmed the presence of Mo. It should be noted that Al and Si peaks are from the SEM stub and Si substrate, respectively.



**Figure 2.** Left: FESEM micrographs of electrospun (a) 15% PEO ultra-fine fibres and (b-d) 15% PEO embedded with different concentrations of  $\text{MoO}_3$  solutions (5%, 7% and 10%). Right: Size distributions of electrospun fibre diameters from SEM images (a-d). Sample with 15% PEO -10%  $\text{MoO}_3$  comprises fibres with diameters above 2000 nm as shown in the inset.



**Figure 3.** (a) High magnification FESEM image (b) size distribution of ultra-fine fibre diameters and (c) EDX spectrum of 15% PEO nanofibres embedded with 10% MoO<sub>3</sub>.

Further increases in the concentration of MoO<sub>3</sub> by mixing 0.1 g of MoO<sub>3</sub> powder with 15% PEO solution significantly improved the quality of fibres (without beads) as shown in Figure 4a. STEM analysis (Figure 4c) shows a uniform distribution of MoO<sub>3</sub> particles inside the fibres. The MoO<sub>3</sub> NPs have been stabilized within the electrospun fibres. EDX mapping of this sample (Figure

5), revealed the presence of  $\text{SiO}_2$  which could be contamination from the glass vial during the solution mixing process using a probe sonicator.

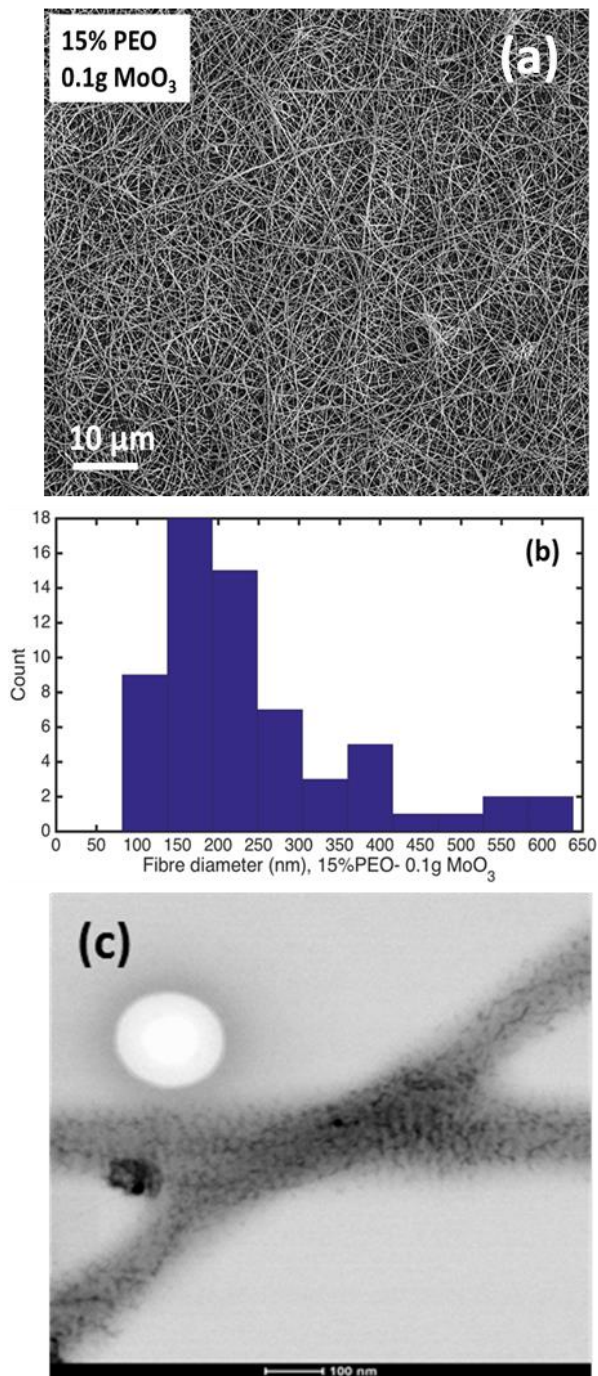


**Figure 4.** (a) SEM image, (b) Size distribution of fibre diameters and (c) STEM image of electrospun nanofibres from a solution of 15% PEO with 0.1 g of  $\text{MoO}_3$  powder using the basic electrospinning setup.

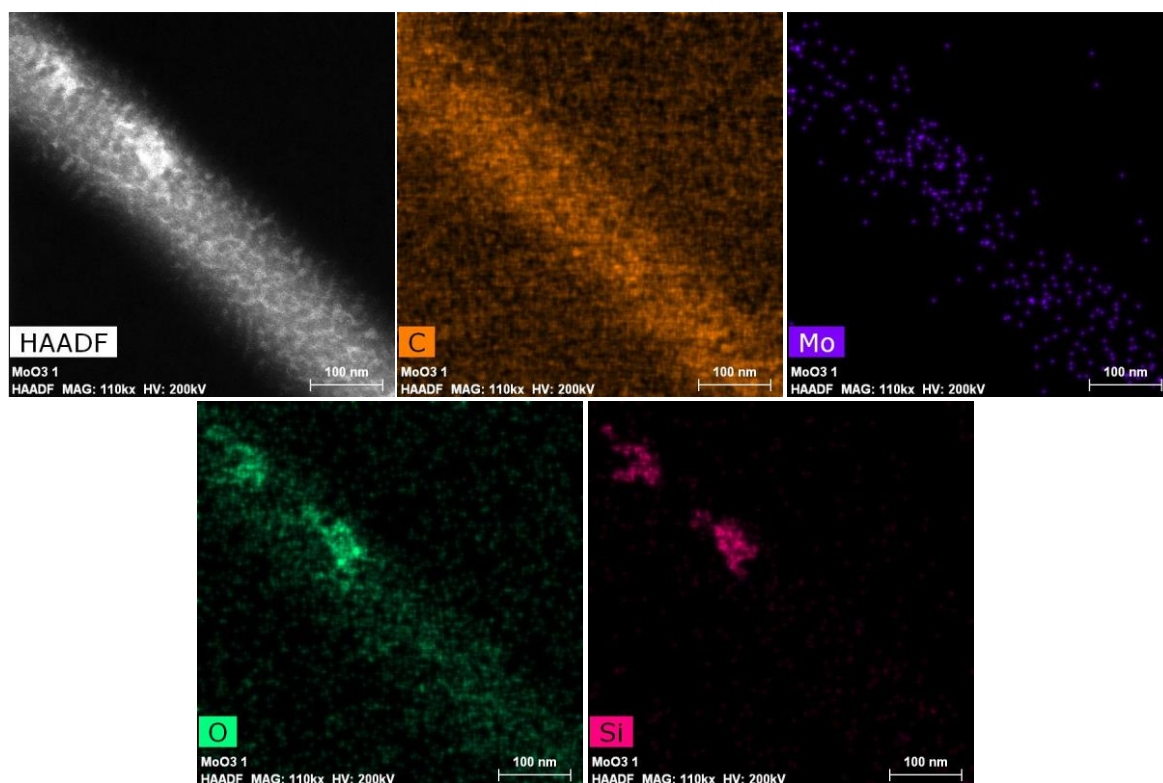


**Figure 5.** STEM image and EDX maps of electrospun PEO nanofibres embedded with MoO<sub>3</sub> particles (15% PEO and 0.1 g MoO<sub>3</sub>)

As mentioned above, the deposition area can be reduced by employing a multiple filed technique, which is attributed to dampening the bending instability [33]. In this work, firstly a metallic ring  $R_t$  (Figure 1) was connected to the tip of needle with the same high voltage as applied to the needle. By the reducing the diameter of the ring (down to 5 cm), we could reduce the deposition area down to 8-9 mm (as shown in Figure 6a). To further reduce the diameter of the deposited area, a second ring,  $R_c$  (Figure 1) was added to the setup. By optimization of the electrospinning parameters as described in the experimental section, the deposition area was significantly reduced to about 4 mm diameter (Figure 6b) as compared to the deposition area of 1 cm diameter reported by Deitzel et al. [33]. This simple modification to the electrospinning process, “controlled electrospinning”, enables precise deposition of nanofibres on small substrates for different applications or for selective deposition of nanofibre mats onto larger substrates.

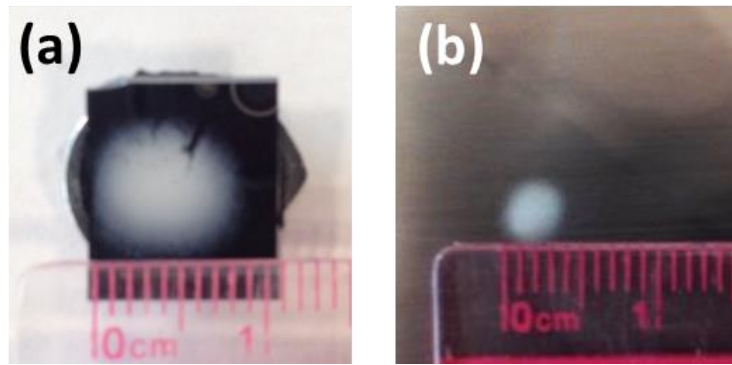


**Figure 6.** Photos of a reduced deposition area from a focused jet using a multi-field technique;

(a) 8-9 mm diameter using one ring and (b) ~4 mm diameter using two rings.

The effect of the secondary voltage of  $R_c$  on the fibre morphology was investigated by SEM. Figure 7a shows a SEM micrograph of the sample with 15% PEO incorporated with 0.1g  $\text{MoO}_3$  powder as electrospun on a Si substrate using the multi-field electrospinning setup. Comparison of the plots for size distribution of fibre diameters for two samples electrospun with basic and multi-field setup (Figures 4b and 7b, respectively) confirm a reduction in fibre diameter. This reduction could be attributed to the higher voltage between the syringe tip and the collector for the multi-field setup compared with the basic setup [33, 34]. When a higher voltage is applied, both columbic forces in the jet and the electric field are stronger. This difference for the multi-field setup results in greater stretching of the solution and a reduction in the fibre diameter [34].

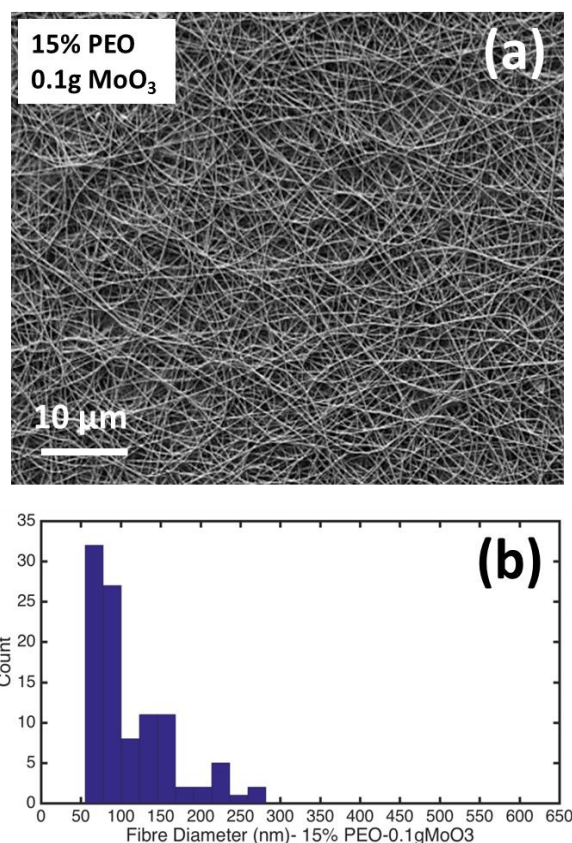


**Figure 7.** a) SEM image and (b) Size distribution of fibre diameters for electrospun nanofibres from a solution of 15% PEO with 0.1 g of MoO<sub>3</sub> powder using a multi-field electrospinning setup.

To further study the nature of the developed electrospun fibres, FT-IR spectra of several samples were measured and are shown in Figure 8. Spectrum (a) was obtained from the pure 15% PEO fibres (Figure 2a) produced using the basic setup. The IR spectrum of PEO has several useful structurally diagnostic features such as the doublet at 1359 and 1342  $\text{cm}^{-1}$  that arises from CH<sub>2</sub> wagging modes and the complex of bands centred at 1101  $\text{cm}^{-1}$  that arise from C-O-C stretching motions of the polymer backbone [35]. The appearance of the CH<sub>2</sub> doublet can be used as an unambiguous measure of crystallinity since the higher wavenumber component decreases in intensity as the crystallinity is decreased with the doublet eventually collapsing to a single mode in amorphous PEO. The C-O-C bands are also sensitive to crystallinity but have also been found to be very responsive to other interactions such as coordination of cations such as K<sup>+</sup> in KBr pellets and Li<sup>+</sup> in PEO-lithium salt electrolytes [35].

The IR spectrum of the 15% PEO + 0.1g of MoO<sub>3</sub> fibres electrospun by the basic setup is shown in Figure 8b. The higher wavenumber component of the CH<sub>2</sub> doublet (1359 cm<sup>-1</sup>) has increased in intensity compared to the previous spectrum indicating the PEO in this sample is more crystalline. This result could be in part due to the larger diameter of these nanofibres, as shown in Figures 4a and b, compared those of the pure 15% PEO shown in Figure 2a. A larger diameter nanofiber provides a greater degree of freedom for polymer chains to rearrange and to align in a more crystalline fashion with drying.

The IR spectrum also reveals changes to the C-O-C band profile that could reflect both an increase in crystallinity and interactions between the C-O-C groups and the MoO<sub>3</sub>. However, it is difficult to tease apart these two effects. Weak bands in the spectrum at 984, 901 and 809 cm<sup>-1</sup> confirm the presence of MoO<sub>3</sub> [36]. The middle band has been shown to exhibit strong LO-TO effects in the order of hundreds of wavenumbers, hence its position is sensitive to the size and morphology of the crystallites. So although the peak at 901 cm<sup>-1</sup> in this sample occurs at considerably higher wavenumbers than is found in larger MoO<sub>3</sub> crystals (~850 cm<sup>-1</sup>), the other bands correspond quite well with peaks of orthorhombic MoO<sub>3</sub>. From the EDX maps in Figure 5, the domain size of the MoO<sub>3</sub> particles appears to be ~10 nm, so the observed wavenumber shift could be a result of the small size of the crystallites, which have nevertheless preserved their orthorhombic structure.

The spectrum in Figure 8c was recorded from the 15% PEO + 0.1g MoO<sub>3</sub> nanofibres produced with the multi-field electrospinning setup. Inspection of the CH<sub>2</sub> doublet reveals that crystallinity has decreased markedly in these fibres, reflecting in part smaller diameters that result from the multi-field setup (Figure 7). However, the MoO<sub>3</sub> must also have a direct effect on the PEO chains, further reducing PEO crystallinity, because the fibre diameters are not markedly smaller than those of the pure PEO. Also the C-O-C band at 1102 cm<sup>-1</sup> has become very strong and sharp; an effect reported previously when the polymer chains interacted strongly with K<sup>+</sup> and Li<sup>+</sup> ions in the cases mentioned above [35]. The exact nature of the interaction is uncertain in this case but the small particle size

and high surface area leave plenty of scope for the oxygen of the polymer ether groups to donate to the incomplete Mo coordination sphere at the MoO<sub>3</sub> crystal domain boundaries.

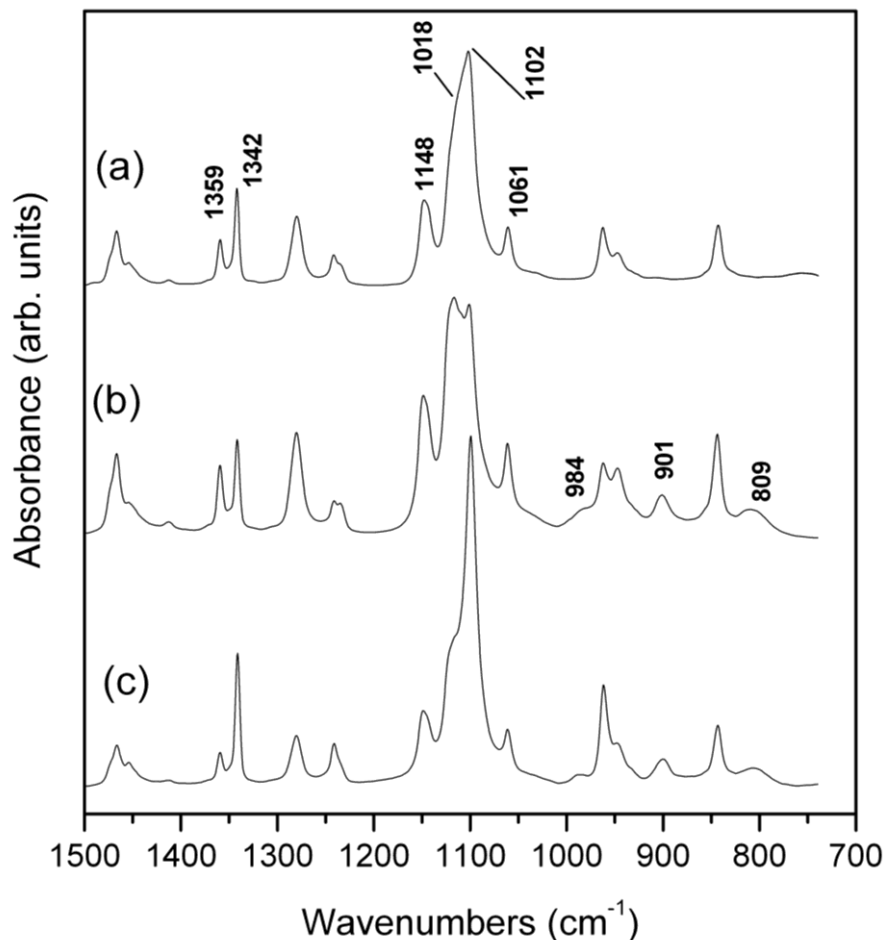


**Figure 8.** FT-IR spectra of (a) 15% PEO and (b) 15% PEO with 0.1 g MoO<sub>3</sub> synthesized by basic electrospinning setup and (c) 15% PEO with 0.1 g MoO<sub>3</sub> electrospun by multi-field technique.

#### 4. Conclusions

We have successfully synthesised high quality ultra-fine fibres embedded with MoO<sub>3</sub> nanoparticles using an electrospinning technique. SEM characterisation revealed that the number of beads and droplets reduces with increased concentration of MoO<sub>3</sub> in solution. STEM analysis showed a uniform distribution of nanoparticles inside the fibres. FT-IR measurements confirmed that the chemical structure of the MoO<sub>3</sub> is preserved in the fibres. FT-IR also indicated that there is a strong interaction between the nanoparticles and the polymer chains, which would help minimise aggregation of nanoparticles. Our simple multi-field electrospinning setup employing two rings

offers control over the location and size of the deposition area down to a few millimetres. These experiments confirmed that a simple direct synthesis of nanoparticle fibres as well as multi-field electrospinning setup offer a cost effective fabrication method for small substrates without the need for organic solvents or subsequent transfer of deposited nanostructures. These electrospun  $\text{MoO}_3$  nanoparticles show high potential for gas sensing applications due to the high surface areas achieved by this preparation process. This simple process also opens up the possibility of synthesizing nanofibres embedded with other metal-oxide nanoparticles as a sensing layer.

### **Acknowledgements**

This work has been supported by the Australian Government, Department of Education through the Endeavour Scholarships and Fellowships programme, QUT Institute for Future Environments (IFE) and Natural Sciences and Engineering Council of Canada. The authors would like to thank Dr Xin Zhang from SFU 4D LABS for assistance in obtaining TEM/STEM images and Mr Zain Khanzada for assistance with the development of the electrospinning setup. The FT-IR measurements were conducted using the IFE Central Analytical Research Facility (CARF).

### **References**

- [1] E. Comini, Metal oxide nano-crystals for gas sensing, *Anal. Chim. Acta.* 568 (2006) 28-40.
- [2] J. Yu, H. Wen, M. Shafiei, M. R. Field, Z. F. Liu, W. Wlodarski, N. Motta, Y. X. Li, K. Kalantar-zadeh, P.T. Lai, A hydrogen/methane sensor based on niobium tungsten oxide nanorods synthesised by hydrothermal method, *Sensor Actuat. B-Chem.* 184 (2013) 118-129.
- [3] M. Shafiei, K. Kalantar-Zadeh, W. Wlodarski, E. Comini, M. Ferroni, G. Sberveglieri, S. Kaciulis, L. Pandolfi, Hydrogen gas sensing performance of Pt/ $\text{SnO}_2$  nanowires/SiC MOS devices, *Int. J. Smart Sens. Intell. Syst.* 1 (2008) 771-783.
- [4] A. H. Khoshaman, P. C. H. Li, N. Merbouh, B. Bahreyni, Highly sensitive supra-molecular thin films for gravimetric detection of methane, *Sensor Actuat. B-Chem.* 161 (2012) 954-960.
- [5] C.-L. Zhang and S.-H. Yu, Nanoparticles meet electrospinning: recent advances and future prospects, *Chem. Soc. Rev.* 43 (2014) 4423-4448.

- [6] M. Shafiei, J. Yu, G. Chen, P. T. Lai, N. Motta, W. Wlodarski, K. Kalantar-zadeh, Improving the hydrogen gas sensing performance of Pt/MoO<sub>3</sub> nanoplatelets using a nano thick layer of La<sub>2</sub>O<sub>3</sub>, *Sensor Actuat. B-Chem.* 187 (2013) 267-273.
- [7] M. Shafiei, J. Yu, M. Breedon, A. Moafi, K. Kalantar-zadeh, W. Wlodarski, R.B. Kaner, K. Galatsis, Pt/MoO<sub>3</sub> nano-flower/SiC Schottky diode based hydrogen gas sensor, *Proceedings of IEEE Sens.* 2010, 354-357.
- [8] M. H. Yaacob, J. Yu, K. Latham, K. Kalantar-zadeh, W. Wlodarski, Optical hydrogen sensing properties of nanostructured Pd/MoO<sub>3</sub> films, *Sensor Lett.* 9 (2011) 16-20.
- [9] W. E. Teo and S. Ramakrishna, A review on electrospinning design and nanofibre assemblies, *Nanotechnology* 17 (2006) R89-R106.
- [10] Y. Guo and Y. Zhou, Polyaniline nanofibers fabricated by electrochemical polymerization: A mechanistic study, *Eur. Polym. J.* 43 (2007) 2292-2297.
- [11] S. Arai, M. Endo, S. Hashizume, Y. Shimojima, Nickel-coated carbon nanofibers prepared by electroless deposition, *Electrochem. Commun.* 6 (2004) 1029-1031.
- [12] B. B. Lakshmi, C. J. Patrissi, C. R. Martin, Sol-gel template synthesis of semiconductor oxide micro- and nanostructures, *Chem. Mater.* 9 (1997) 2544-2550.
- [13] S. A. Moshkalyov, A. L. D. Moreau, H. R. Gutiérrez, M. A. Cotta, J. W. Swart, Carbon nanotubes growth by chemical vapor deposition using thin film nickel catalyst, *Mater. Sci. Eng. B*, 112 (2004) 147-153.
- [14] R. V. Parthasarathy, K. L. N. Phani, C. R. Martin, Template synthesis of graphitic nanotubules, *Adv. Mater.* 7 (1995) 896-897.
- [15] G. M. Kim, S. M. Lee, G. H. Michler, H. Roggendorf, U. Gösele, M. Knez, Nanostructured pure anatase titania tubes replicated from electrospun polymer fiber templates by atomic layer deposition, *Chem. Mater.* 20 (2008) 3085-3091.
- [16] C. Shao, X. Yang, H. Guan, Y. Liu, J. Gong, Electrospun nanofibers of NiO/ZnO composite, *Inorg. Chem. Commun.* 7 (2004) 625-627.

- [17] Z. Liu, D. D. Sun, P. Guo, J. O. Leckie, An efficient bicomponent  $\text{TiO}_2/\text{SnO}_2$  nanofiber photocatalyst fabricated by electrospinning with a side-by-side dual spinneret method, *Nano Lett.* 7 (2007) 1081-1085.
- [18] D. Li and Y. Xia, Direct fabrication of composite and ceramic hollow nanofibers by electrospinning, *Nano Lett.* 4 (2004) 933-938.
- [19] K. K. H. Wong, M. Zinke-Allmang, J. L. Hutter, S. Hrapovic, J. H. T. Luong, W. Wan, The effect of carbon nanotube aspect ratio and loading on the elastic modulus of electrospun poly(vinyl alcohol)-carbon nanotube hybrid fibers, *Carbon* 47 (2009) 2571-2578.
- [20] D. Crespy, K. Friedemann, A.-M. Popa, Colloid-electrospinning: fabrication of multicompartiment nanofibers by the electrospinning of organic or/and inorganic dispersions and emulsions, *Macromol. Rapid Comm.* 33 (2012) 1978-1995.
- [21] P.-C. Hsu, H. Wu, T. J. Carney, M. T. McDowell, Y. Yang, E. C. Garnett, M. Li, L. Hu, Y. Cui, Passivation coating on electrospun copper nanofibers for stable transparent electrodes, *ACS Nano* 6 (2012) 5150-5156.
- [22] A. S. Badami, M. R. Kreke, M. S. Thompson, J. S. Riffle, A. S. Goldstein, Effect of fiber diameter on spreading, proliferation, and differentiation of osteoblastic cells on electrospun poly(lactic acid) substrates, *Biomaterials* 27 (2006) 596-606.
- [23] W. Shi, S. Song, H. Zhang, Hydrothermal synthetic strategies of inorganic semiconducting nanostructures, *Chem. Soc. Rev.* 42 (2013) 5714-5743.
- [24] A.-L. Reysenbach and E. Shock, Merging genomes with geochemistry in hydrothermal ecosystems, *Science* 296 (2002) 1077-1082.
- [25] X. F. Lu, Y. Y. Zhao, C. Wang, Fabrication of PbS nanoparticles in polymer-fiber matrices by electrospinning, *Adv. Mater.* 17 (2005) 2485-2488.
- [26] H. Al-Kandari, F. Al-Khorafi, H. Belatel, A. Katrib, The bifunctional catalytic properties of a partially  $\text{H}_2$ -reduced  $\text{MoO}_3$ , *Catal. Commun.* 5 (2004) 225-229.

- [27] M. A. Quevedo-Lopez, R. F. Reidy, R. A. Orozco-Teran, O. Mendoza-Gonzalez, R. Ramirez-Bon, Enhancement of the photochromic and thermochromic properties of molybdenum oxide thin films by a cadmium sulfide underlayer, *J. Mater. Sci.: Mater. Elec.* 11 (2000) 151-155.
- [28] J. Yu, J. Liu, M. Breedon, M. Shafiei, H. Wen, Y. X. Li, W. Wlodarski, G. Zhang, K. Kalantar-zadeh, The correlation between electric field emission phenomenon and Schottky contact reverse bias characteristics in nanostructured systems, *J. Appl. Phys.* 109 (2011) 114316.
- [29] C. Feng, H. Gao, C. Zhang, Z. Guo, H. Liu, Synthesis and electrochemical properties of  $\text{MoO}_3/\text{C}$  nanocomposite, *Electrochim. Acta.* 93 (2013) 101-106.
- [30] S. Li, C. Shao, Y. Liu, S. Tang, R. Mu, Nanofibers and nanoplatelets of  $\text{MoO}_3$  via an electrospinning technique, *J. Phys. Chem. Solids.* 67 (2006) 1869-1872.
- [31] P. Gouma, Nanostructured polymorphic oxides for advanced chemosensors, *Rev. Adv. Mater. Sci.* 5 (2003) 147-154.
- [32] P. Gouma, K. Kalyanasundaram, A. Bishop, Electrospun single-crystal  $\text{MoO}_3$  nanowires for biochemistry sensing probes, *Mater. Res. S.* 21 (2006) 2904-2910.
- [33] J. M. Deitzel, J. D. Kleinmeyer, J. K. Hirvonen, N. C. Beck Tan, Controlled deposition of electrospun poly(ethylene oxide) fibers, *Polymer.* 42 (2001) 8163-8170.
- [34] N. Bhardwaj and S. C. Kundu, Electrospinning: A fascinating fiber fabrication technique, *Biotechnol. Adv.* 28 (2010) 325-347.
- [35] I. Pucić and T. Jurkin, FTIR assessment of poly(ethylene oxide) irradiated in solid state, melt and aqueous solution, *Radiat. Phys. Chem.* 81 (2012) 1426-1429.
- [36] L. Sequin, M. Figlarz, R. Cavagnat, J.-C. Lassègues, Infrared and Raman spectra of  $\text{MoO}_3$  molybdenum trioxides and  $\text{MoO}_3 \cdot x\text{H}_2\text{O}$  molybdenum trioxide hydrates, *Spectrochimic Acta. A.* 51 (1995) 1323-1344.